Resonant enhancement of the zero-phonon emission from a colour centre in a diamond cavity

Andrei Faraon[1]*, Paul E. Barclay[1,2,3], Charles Santori[1], Kai-Mei C. Fu[1,4] and Raymond G. Beausoleil[1]

Integrated quantum photonic technologies are key for future applications in quantum information[1,2], ultralow-power opto-electronics[3] and sensing[4]. As individual quantum bits, nitrogen-vacancy centres in diamond are among the most promising solid-state systems identified to date, because of their long-lived electron and nuclear spin coherence, and capability for individual optical initialization, readout and information storage[5–9]. The major outstanding hurdle lies in interconnecting many nitrogen vacancies for large-scale computation. One of the most promising approaches in this regard is to couple them to optical resonators, which can be further interconnected in a photonic network[10–12]. Here, we demonstrate coupling of the zero-phonon line of individual nitrogen vacancies to the modes of microring resonators fabricated in single-crystal diamond. Zero-phonon line enhancement by more than a factor of 10 is estimated from lifetime measurements. The devices are fabricated using standard semiconductor techniques and off-the-shelf materials, thus enabling integrated diamond photonics.

Previous efforts to couple nitrogen-vacancy (NV) centres to optical resonators have been hindered by difficulties in the fabrication of single-crystal diamond[13–15] or integration of diamond with other optical materials[16–18]. Coupling to microresonators has been observed using diamond nanoparticles, but the spectral and coherence properties of NVs in these structures are not suitable for quantum information applications[19–22]. Enhanced zero-phonon line (ZPL) emission by coupling to surface plasmons[23,24] has recently been reported; however, in those cases both the ZPL and phonon sidebands are enhanced. In our approach, the resonator is fabricated directly in a single-crystal diamond membrane, thus enabling selective enhancement of the ZPL while the emission rate into the phonon sidebands remains almost unchanged. By using single-crystal diamond it is expected that NV centres with excellent spectral properties could be integrated into an optical quantum network.

The spontaneous emission rate enhancement of a particular dipole transition i of an emitter coupled to a microresonator, relative to the uniform dielectric medium of the resonator, is enhanced[25] by the factor $(\tau_0/\tau_{\text{leak}})_i + F_i$, where $1/\tau_0$ is the emission rate in the uniform dielectric medium, $1/\tau_{\text{leak}}$ is the emission rate outside the cavity mode, and

$$F_i = F_{\text{cav}} \left(\frac{\mathbf{E}(\mathbf{r}_i) \cdot \boldsymbol{\mu}_i}{|\mathbf{E}_{\text{max}}||\boldsymbol{\mu}_i|} \right)^2 \frac{1}{1 + 4Q^2(\lambda_i/\lambda_{\text{cav}} - 1)^2} \qquad (1)$$

where $\boldsymbol{\mu}_i$ is the dipole moment, $\mathbf{E}(\mathbf{r}_i)$ is the local electric field at the emitter location $\mathbf{r}_i$, λ_{cav} is the cavity wavelength, λ_i is the emitter wavelength, and $|\mathbf{E}_{\text{max}}|$ is the maximum value of the electric field

in the resonator. For the case where the dipole is resonant with the cavity and also ideally positioned and oriented with respect to the local electric field, $F = F_{\text{cav}}$, where

$$F_{\text{cav}} = \frac{3}{4\pi^2} \left(\frac{\lambda_{\text{cav}}}{n} \right)^3 \frac{Q}{V_{\text{mode}}} \qquad (2)$$

and $V_{\text{mode}} = \left(\int_V \epsilon(\mathbf{r})|\mathbf{E}(\mathbf{r})|^2 d^3\mathbf{r} \right) / \max\left(\epsilon(\mathbf{r})|\mathbf{E}(\mathbf{r})|^2 \right)$ is the optical mode volume of the resonator, and $\epsilon(\mathbf{r})$ is the electric permittivity at position $\mathbf{r}$.

The optical cavity used in the experiment consisted of a diamond microring on a silicon dioxide pedestal (Fig. 1). The microring, 4.8 μm in diameter and 700 nm wide, was etched into
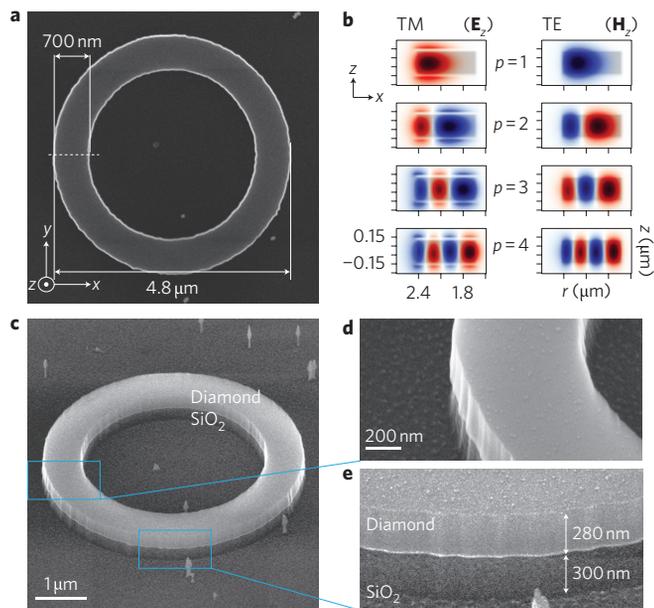

Figure 1 | Microring resonator fabricated in single-crystal diamond. a, Scanning electron microscope image of the device (top view). The dashed line indicates the location of the azimuthal cross-section for which the fields in **b** are plotted. **b**, Simulated field profile (azimuthal cross-section) of the TM$_{m=40}$ (**E**$_z$ component shown, where the index z indicates the direction perpendicular to the plane of the ring) and TE$_{m=40}$ (**H**$_z$ field component shown) resonances supported by this microring. (m is the azimuthal quantum number and p is the radial quantum number.) **c–e**, Side view of the microdisk, showing surface roughness arising from the fabrication process. In **e** it can be seen how the 2-μm-thick SiO$_2$ substrate has also been etched by 300 nm during the fabrication process (with the diamond ring acting as a mask).

[1]Hewlett Packard Laboratories, 1501 Page Mill Road, Palo Alto, California 94304, USA, [2]Institute for Quantum Information Science and Department of Physics and Astronomy, University of Calgary, Calgary, Alberta, Canada, [3]National Institute for Nanotechnology, Edmonton, Alberta, Canada, [4]Department of Physics, University of Washington, Seattle, Washington 98195, USA. *e-mail: andrei.faraon@hp.com
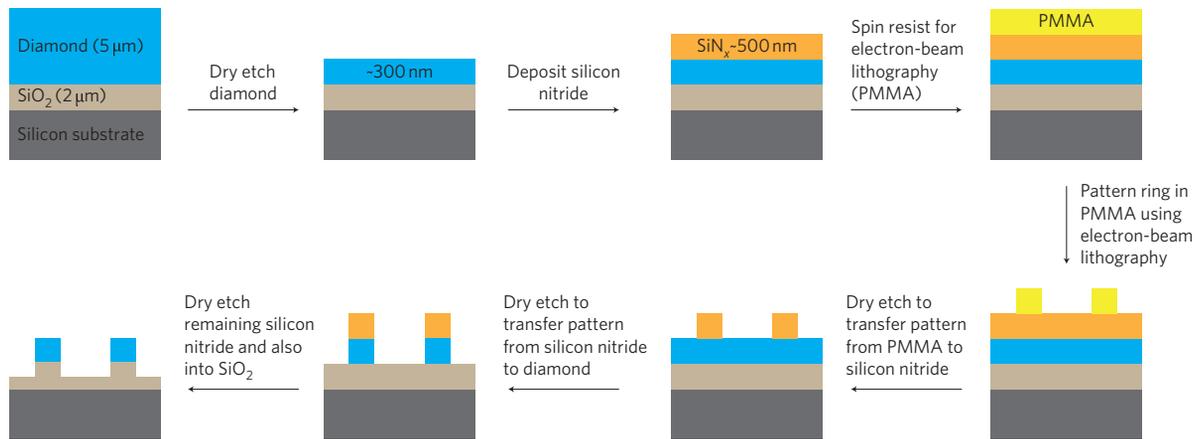
Figure 2 | Schematic (not to scale) showing the sequence of fabrication steps. A 5 µm-thick diamond membrane was located on a 2-µm-thick thermal SiO$_2$ layer grown on a silicon wafer. No special mounting procedure was used to attach the membrane to the substrate. The fabrication steps were as follows. (1) Dry etching (oxygen plasma in an Oxford RIE etching machine) was used to thin the membrane until it was ~280 nm-thick. (2) A 500-nm-thick silicon nitride layer was deposited on top of the chip using an Oxford PECVD machine. (3) Electron-beam resist (PMMA 495 K A8) was spun on the chip and electron-beam lithography was used to pattern the ring in the resist. (4) The pattern was transferred from the resist to the silicon nitride by means of dry etching (SF$_6$/C$_4$F$_8$ chemistry). (5) The pattern was transferred from the silicon nitride to the diamond using dry etching in oxygen plasma. This step also removed any remaining resist mask. (6) Finally, the remaining silicon nitride mask was removed as in Step 4. This etching step also etched ~300 nm into the SiO$_2$ substrate.

a 280-nm-thick diamond membrane that was obtained by thinning a 5-µm-thick type IIa single-crystal diamond membrane (purchased already polished to 5 µm from Element 6) using reactive ion etching (RIE) in an oxygen plasma. During the etching process (outlined in Fig. 2), the membrane was mounted on a 2 µm-thick SiO$_2$ substrate thermally grown on a silicon wafer. After membrane preparation, a silicon nitride layer (500 nm) was deposited on top, and the ring was patterned in this layer using electron-beam lithography and RIE. Two more etching steps were used to transfer the pattern from the silicon nitride to the diamond and then to remove any excess silicon nitride. During the final RIE step, the oxide substrate was also etched by 300 nm. The resulting construction is a multimode resonator that supports four radial transverse magnetic (TM) modes and four transverse electric (TE) modes with the electromagnetic field profile shown in Fig. 1b (simulated using the MEEP software package developed at MIT). The simulated quality factor Q can exceed 1×10^6, but for the device used in this experiment the quality factor was limited to 5,000 by imperfections in the fabrication process (mainly the surface roughness shown in Fig. 1d,e). These values of Q are much higher than those observed in microresonators fabricated in nanocrystalline diamond[26]. The optical mode volume ranges from $V_{mode} \approx 17(\lambda/n)^3$ to $V_{mode} \approx 32(\lambda/n)^3$ depending on the particular standing wave mode, where λ is the resonance wavelength in air and $n = 2.4$ is the index of refraction of diamond. Our simulations indicate the smallest mode volumes for fundamental TE/TM radial modes ($p = 1$) with azimuthal quantum number $m = 46$ at $\lambda_{cav} = 637$ nm.

During the experiment, the sample was cooled to below 10 K in a continuous-flow liquid-helium cryostat. A confocal microscope set-up was used for optical excitation and collection from the top of the ring. The NV centres studied were present in the original membrane, having been incorporated accidentally during diamond growth. The photoluminescence spectrum while pumping the microdisk with a continuous-wave green laser (532 nm, 2 mW) is shown in Fig. 3a. As well as the diamond Raman line, the ZPLs and phonon sidebands from both the neutral (NV^0) and negatively charged (NV$^-$) centres are visible in the spectrum, and multiple cavity modes can be observed on top of the phonon sidebands. A higher-resolution spectrum (Fig. 3b) shows that the laser spot with an area of 1 µm^2 excites about ten distinct NV$^-$ ZPLs

distributed over ~1 nm (~1 THz) because of strain in the sample[27]. This strain-induced inhomogeneous broadening was not present in the initial 5 µm membrane, which exhibits an ensemble ZPL with an ~20 GHz linewidth. Two resonant modes, C1 and C2, with quality factors Q1 = 4,300 and Q2 = 3,800 are spectrally detuned by only a few nanometres from the ZPL at 637 nm (Fig. 3b). Considering a quality factor of $Q = 4,000$, the maximum expected enhancement factor for an optical dipole ideally aligned and positioned with respect to the local electric field ranges from $1 + F \approx 10$ to $1 + F \approx 19$. Here, and in the rest of this Letter, we assume $\tau_0/\tau_{leak} = 1$, based on our experimental finding that the total decay rate into modes outside the cavity ($1/\tau_{leak}$) is approximately equal to the total decay rate in bulk diamond $1/\tau_0 \approx (12 \text{ ns})^{-1}$.

The modes of the microdisk could be redshifted by injecting xenon gas into the cryostat[28]. The xenon condensed on the resonator, thereby increasing the effective microring size and resulting in a resonance shift (Fig. 3c). The flow rate of xenon inside the cryostat was not constant while the data for Fig. 3c were being collected, so there is no well-defined correspondence between the resonance shift and scan number. The resonance shift can also be used to distinguish between the spectral lines corresponding to cavity modes and the NV lines. When modes C1 and C2 are tuned over the ZPL, a few NV lines show strong intensity enhancement, a signature of coupling to the cavity (Fig. 3c–e). More ZPL photoluminescence is collected in the coupled case, because the enhanced NV emits more photons in the ZPL, and also because these photons are coupled into the mode of the ring that scatters out of plane from sidewall roughness. One of the NV lines, marked NV1, couples to both C1 and C2. These two modes tune at the same rate and have roughly the same quality factor, suggesting that they represent standing waves formed from counter-propagating modes of the same radial and azimuthal order, coupled through surface roughness scattering. The position of the scattering centres also defines the spatial position of the standing waves. Enhancement of the collected photoluminescence depends not only on the emission rate of photons into the cavity mode, but also on the collection efficiency for light emitted into the cavity, and then scattered out. To obtain a more quantitative estimate of the rate of photon emission into the cavity, we performed photoluminescence lifetime measurements as described below.
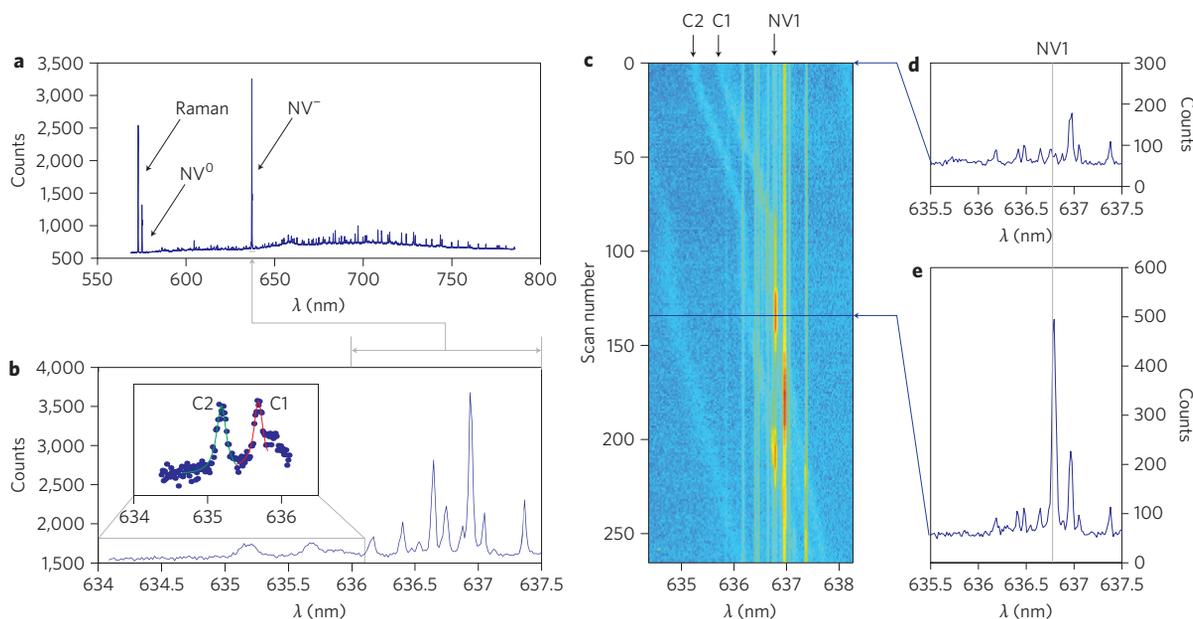
Figure 3 | Spectral characterization showing enhanced NV photoluminescence due to coupling to the cavity mode. a, Broadband photoluminescence spectrum under continuous-wave excitation. Raman scattering and the ZPL from NV^0 and NV^- are marked on the spectrum. Multiple cavity modes can be observed in the phonon sidebands. **b,** Higher-resolution spectrum over the NV^- ZPL region shows two modes, C1 and C2, blue detuned by only a few nanometres from the ZPL. The quality factors are Q1 = 4,300 and Q2 = 3,800 (see inset). **c,** When tuning C1 and C2 over the ZPL, a few NVs exhibit enhanced emission. The tuning rate was reduced when C1 and C2 crossed the ZPL. The transition labelled 'NV1' couples to both C1 and C2. The colour plot was generated using a logarithmic scale. **d,e,** Spectra of NV1 in uncoupled (**d**) and coupled (**e**) cases.
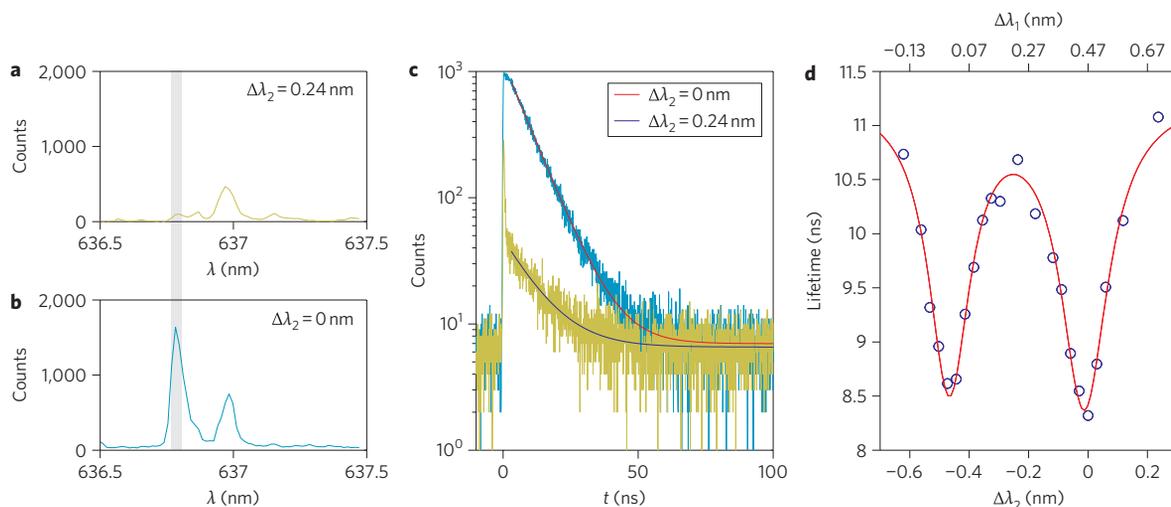

Figure 4 | Lifetime measurements for NV1. a,b, Photoluminescence spectrum of NV1 under pulsed excitation when coupled to C2 ($\Delta\lambda_2 = 0$ nm) (**b**) and uncoupled ($\Delta\lambda_2 = 0.24$ nm) (**a**). The grey bar marks the spectral filter window used to collect only photons emitted in the NV1 ZPL. **c,** Lifetime measurement for uncoupled ($\tau_0 = 11.1$ ns, $\Delta\lambda_2 = 0.24$ nm) and coupled ($\tau_{c2} = 8.3$ ns, $\Delta\lambda_2 = 0$) cases. **d,** Change in lifetime as C1 and C2 are tuned over the NV1 ZPL. The data are well fit (red line) assuming coupling to two cavity modes with quality factors Q1 = 4,300 and Q2 = 3,800, as measured from the spectra, and considering that the emission rate into each cavity mode follows a Lorentzian dependence with respect to detuning.

Lifetime measurements were performed using a green pulsed excitation with a repetition rate of 4.75 MHz, using a filtered supercontinuum source (520 nm centre wavelength; 28 nm bandwidth; 200 μW). The pulsed excitation spectra of NV1, both in the uncoupled case and when coupled to C2, are shown in Fig. 4a,b. As expected, under pulsed excitation, more photons are collected from NV1 when coupled to the cavity. A monochromator was used to spectrally filter (0.03 nm ≈ 20 GHz bandwidth) only the NV1 ZPL, and the filtered signal was sent to a photon counter. The temporal profile of the photoluminescence emission was

fitted by a single exponential function (Fig. 4c), indicating a change in the NV1 lifetime from $\tau_0 = 11.1$ ns in the uncoupled case to $\tau_{c2} = 8.3$ ns when resonant with cavity mode C2. Note that the first 3 ns following the excitation pulse were skipped in the fits shown in Fig. 4c to minimize the influence of fast luminescence arising from any contamination on the sample acquired during sample processing. If the total photon emission rate for uncoupled NVs is $1/\tau_0 = 1/\tau_{ZPL} + 1/\tau_{PS}$, in the coupled case the rate becomes $1/\tau_{c2} = (1 + F)/\tau_{ZPL} + 1/\tau_{PS}$, where F, $1/\tau_{ZPL}$ and $1/\tau_{PS}$ are the Purcell factor and the spontaneous emission rates
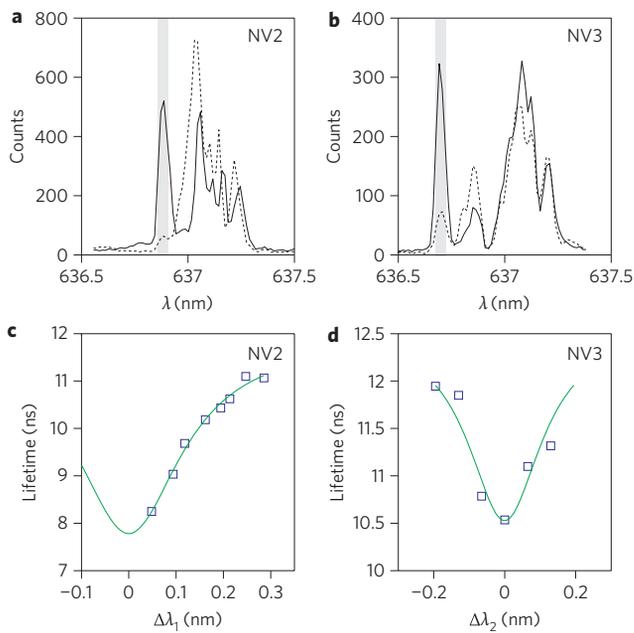
Figure 5 | Lifetime measurements for NV2 and NV3. a,b, Photoluminescence spectra for NV2 (**a**) and NV3 (**b**) under pulsed excitation both for cavity on resonance with the NV line (continuous line), and the cavity off resonance with the NV line (dashed line). The grey bar shows the spectral filter for the NV ZPL. **c,d,** Lifetime as a function of detuning from the cavity mode for NV2 (**c**) and NV3 (**d**).

into the ZPL and phonon sidebands, respectively. The Purcell factor is then given by $F = (\tau_0/\tau_{c2} - 1)/\xi_{ZPL}$, where ξ_{ZPL} is the branching ratio into the ZPL ($\xi_{ZPL} = \tau_0/\tau_{ZPL}$). Our own measurements on other diamond samples indicate a branching ratio of $\xi_{ZPL} \approx 0.03$, while other sources report values ranging from $\xi_{ZPL} \approx 0.024$ (ref. 29; determined from absorption measurements) to $\xi_{ZPL} \approx 0.05$ (ref. 30). A branching ratio of $\xi_{ZPL} \approx 0.03$ gives a total enhancement factor $1 + F \approx 12$. This estimate neglects any possible non-radiative decay channels that may also be present. If such non-radiative decay occurs, then the true ZPL enhancement factor could be even higher than the one estimated here. The lifetime of NV1 was also measured at different detunings from C1 and C2, as shown in Fig. 4d. Decreased lifetimes are observed when both C1 and C2 cross over the NV1 resonance. The fit in Fig. 4d shows that the change in lifetime follows the expected tuning dependence (equation (1)) for a dipole coupled to two cavity modes with quality factors Q1 = 4,300 and Q2 = 3,800 (as measured from the photoluminescence spectra).

Other NV lines on this sample showed coupling to cavity modes, as shown in Fig. 5, for the same microring device. While NV2 was coupled to C1 and showed a similar lifetime reduction as NV1, NV3 was coupled to C2 and on resonance the lifetime was reduced by a relatively smaller amount (10.4 ns minimum lifetime). We note that the pulsed photoluminescence spectra in Fig. 5a,b show a higher concentration of NV$^-$ than in Figs 4a,b. This difference occurred because the measurements in Figs 5 and 4 were performed before and after, respectively, the sample was imaged with a scanning electron microscope, which caused some conversion from NV$^-$ to NV^0.

The measured spontaneous emission rate enhancement of 12 is smaller than the maximum expected from simulations, because of the non-ideal placement and orientation of the NV with respect to the standing wave. With an enhancement factor of 12, the ZPL branching ratio changes from 3/100 to 36/133 ($\sim$25%). With the same resonator design the branching ratio could exceed 98% for

$Q > 5 \times 10^5$. This improvement in Q should be possible with improved fabrication processing (better techniques for cleaning and etching the membrane, use of higher purity material). Branching ratios exceeding 99.5%, as needed for quantum computing protocols, are possible using photonic crystals with $V_{mode} \approx 2(\lambda/n)^3$ and $Q > 2 \times 10^5$ (ref. 31).

Coupling single NV centres to single-crystal diamond resonators is a first critical step towards large-scale integrated diamond quantum optical networks. In the near term, improvements in fabrication processes should yield structures with higher Q, and allow integration of both low-loss waveguides and more complex optical elements such as switches and directional couplers, similar to those in on-chip silicon optical interconnects. Studies of the optical manipulation and coherence of single NV spins in cavities will require centres with high-quality spectral properties located at optimal positions with respect to cavity modes. Therefore, in parallel it will be important to develop methods to place NV centres at predetermined positions and orientations on a diamond chip[32], without introducing additional point defects, and to release the sample strain to reduce inhomogeneous broadening. Even relatively simple chip-scale quantum networks could enable quantum simulators that would significantly outperform classical computers in applications such as quantum chemistry[33]. These devices, operating at the fundamental limit of light–matter interaction could also enable future optical signal-processing devices and sensors operating at ultralow power levels, as well as provide a platform for fundamental studies of many-particle entanglement, which is a prerequisite of non-trivial quantum factoring and searching[1].

Methods
Procedure for sample fabrication. The fabrication process is shown schematically in Fig. 2.

References
1. Nielsen, M. A. & Chuang, I. L. *Quantum Computation and Quantum Information* (Cambridge Univ. Press, 2000).
2. O'Brien, J. L., Furusawa, A. & Vučković, J. Photonic quantum technologies. *Nature Photon.* **3,** 687–695 (2009).
3. Mabuchi, H. Cavity-QED models of switches for attojoule-scale nanophotonic logic. *Phys. Rev. A* **80,** 045802 (2009).
4. Balasubramanian, G. *et al.* Nanoscale imaging magnetometry with diamond spins under ambient conditions. *Nature* **455,** 648–651 (2008).
5. Jelezko, F. *et al.* Observation of coherent oscillation of a single nuclear spin and realization of a two-qubit conditional quantum gate. *Phys. Rev. Lett.* **93,** 130501 (2004).
6. Balasubramanian, G. *et al.* Ultralong spin coherence time in isotopically engineered diamond. *Nature Mater.* **8,** 383–387 (2009).
7. Santori, C. *et al.* Coherent population trapping of single spins in diamond under optical excitation. *Phys. Rev. Lett.* **97,** 247401 (2006).
8. Buckley, B. B., Fuchs, G. D., Bassett, L. C. & Awschalom, D. D. Spin-light coherence for single-spin measurement and control in diamond. *Science* **330,** 1212–1215 (2010).
9. Gurudev Dutt, M. V. *et al.* Quantum register based on individual electronic and nuclear spin qubits in diamond. *Science* **316,** 1312–1316 (2007).
10. Cabrillo, C., Cirac, J. I., García-Fernández, P. & Zoller, P. Creation of entangled states of distant atoms by interference. *Phys. Rev. A* **59,** 1025–1033 (1999).
11. Childress, L., Taylor, J. M., Sørensen, A. S. & Lukin, M. D. Fault-tolerant quantum repeaters with minimal physical resources and implementations based on single-photon emitters. *Phys. Rev. A* **72,** 052330 (2005).
12. Togan, E. *et al.* Quantum entanglement between an optical photon and a solid-state spin qubit. *Nature* **466,** 730–734 (2010).
13. Wang, C. F., Hu, E. L., Yang, J. & Butler, J. E. Fabrication of suspended single crystal diamond devices by electrochemical etch. *J. Vac. Sci. Technol. B* **25,** 730–733 (2007).
14. Greentree, A. *et al.* Critical components for diamond-based quantum coherent devices. *J. Phys. Condens Matter* **18,** S825–S842 (2006).
15. Babinec, T. M., Choy, J. T., Smith, K. J. M., Khan, M. & Loncar, M. Design and focused ion beam fabrication of single crystal diamond nanobeam cavities. *J. Vac. Sci. Technol. B* **29,** 010601 (2011).

16. Larsson, M., Dinyari, K. N. & Wang, H. Composite optical microcavity of diamond nanopillar and silica microsphere. *Nano Lett.* **9,** 1447–1450 (2009).

17. Fu, K.-M. C. *et al.* Coupling of nitrogen-vacancy centers in diamond to a gap waveguide. *Appl. Phys. Lett.* **93,** 234107 (2008).

18. Barclay, P. E., Fu, K-M. C., Santori, C. & Beausoleil, R. G. Chip-based microcavities coupled to nitrogen-vacancy centers in single crystal diamond. *Appl. Phys. Lett.* **95,** 191115 (2009).

19. Wolters, J. *et al.* Enhancement of the zero phonon line emission from a single nitrogen vacancy center in a nanodiamond via coupling to a photonic crystal cavity. *Appl. Phys. Lett.* **97,** 141108 (2010).

20. Barclay, P. E., Santori, C., Fu, K.-M., Beausoleil, R. G. & Painter, O. Coherent interference effects in a nano-assembled diamond NV center cavity-QED system. *Opt. Express* **17,** 8081–8097 (2009).

21. Park, Y-S., Cook, A. K. & Wang, H. Cavity QED with diamond nanocrystals and silica microspheres. *Nano Lett.* **6,** 2075–2079 (2006).

22. Englund, D. *et al.* Deterministic coupling of a single nitrogen vacancy center to a photonic crystal cavity. *Nano Lett.* **10,** 3922–3926 (2010).

23. Kolesov, R. *et al.* Wave particle duality of single surface plasmon polaritons. *Nature Phys.* **5,** 470–474 (2009).

24. Schietinger, S., Barth, M., Aichele, T. & Benson, O. Plasmon-enhanced single photon emission from a nanoassembled metal-diamond hybrid structure at room temperature. *Nano Lett.* **9,** 1694–1698 (2009).

25. Purcell, E. M. Spontaneous emission probabilities at radio frequencies. *Phys. Rev.* **69,** 681 (1946).

26. Wang, C. F. *et al.* Fabrication and characterization of two-dimensional photonic crystal microcavities in nanocrystalline diamond. *Appl. Phys. Lett.* **91,** 201112 (2007).

27. Davies, G. & Hamer, M. F. Optical studies of the 1.945 eV vibronic band in diamond. *Proc. R. Soc. Lond. A* **348,** 285–298 (1976).

28. Mosor, S. *et al.* Scanning a photonic crystal slab nanocavity by condensation of xenon. *Appl. Phys. Lett.* **87,** 141105 (2005).

29. Davies, G. Vibronic spectra in diamond. *J. Phys. C* **7,** 3797–3809 (1974).

30. Siyushev, P. *et al.* Low-temperature optical characterization of a near-infrared single-photon emitter in nanodiamonds. *New J. Phys.* **11,** 113029 (2009).

31. Tomljenovic-Hanic, S., Greentree, A. D., de Sterke, C. M. & Prawer, S. Flexible design of ultrahigh-Q microcavities in diamond-based photonic crystal slabs. *Opt. Express* **17,** 6465–6475 (2009).

32. Toyli, D. M., Weis, C. D., Fuchs, G. D., Schenkel, T. & Awschalom, D. D. Chip-scale nanofabrication of single spins and spin arrays in diamond. *Nano Lett.* **10,** 3168–3172 (2010).

33. Lanyon, B. P. *et al.* Towards quantum chemistry on a quantum computer. *Nature Chem.* **2,** 106–111 (2010).

Acknowledgements

Additional information

The authors declare no competing financial interests. Reprints and permission information is available online at http://www.nature.com/reprints/. Correspondence and requests for materials should be addressed to A.F.